Sensors & Transducers, Vol. 157, Issue 10, October 2013, pp. 234-239

www.sensorsportal.com

Sensors & Transducers

http://www.sensorsportal.com

A Large-Scale Particle Image Velocimetry System Based on Dual-camera Field of View Stitching

[1] Fengzhou Wang, [2] Baohua Xu, [3] Mengxi Xu, [3] Jianqiang Shi, [1] Lang Jia, [*1] Chenming Li

[1] College of Computer and Information Engineering, Hohai University, Nanjing 211100, P. R. China
[2] Yangtze River Estuary Survey Bureau of Hydrology and Water Resource CWRC, Ministry of Water Resources, Shanghai 200136, P. R. China
[3] School of Computer Engineering, Nanjing Institute of Technology, Nanjing 211167, P. R. China
[*] Tel.: +86 25 58099120, fax: +86 25 58099120
[*] E-mail: banjamin2008@163.com, hhice@126.com

Received: 11 July 2013 /Accepted: 25 October 2013 /Published: 31 October 2013

Abstract: Large-Scale Particle Image Velocimetry (LSPIV) is an effective method for the measurement of the river surface flow velocity. For the wide cross-section river, in the near-field area of river surface image there are small and clear targets. But the flow tracers are almost invisible in the far-field area because of the resolution limit of one single video camera, which makes it difficult to complete the velocimetry task. So a dual-camera based LSPIV system has been developed for monitoring the wide cross-section river. This system is based on two digital Internet Protocol (IP) video cameras either of which captures more than half of the river surface with high resolution. And then the developed system stitches the two images into one covering the entire wide cross-section rivers. In the far field of river, the accuracy of the vector increases from 20.4 % to 80.4 %.

Keywords: River flow velocity measurement, Large scale particle image velocimetry, Dual-camera, Image stitching.

1. Introduction

Particle Image Velocimetry (PIV) was developed in the late seventies as a transient, multi-point, non-contact method of hydrodynamic velocity, which makes up the limitations of single-point velocimetry measurement. But for the large-scale flow measurements, PIV cannot cover the entire scenes, so Fujita [1] proposed a Large-Scale Particle Image Velocimetry (LSPIV) method.

Conventional LSPIV system is a shore-based system which captures images by one single video camera. In the near-field area of river surface image there are small and clear targets, but the flow tracers are almost invisible in the far-field area because of the resolution limit of one single video camera, especially for those rivers which flow area up to thousands of square meters. The low resolution images of the far-field will lead to high error rate of motion estimation.

To address these problems, Fujita *et al.* [2] got the vertical viewing and stitched the flow field image of the downstream direction by helicopters. But it could only observe the surface of the large-scale. Bechle *et al.* [3] shot the river near-field and far-field using two video cameras, but he did not mention the

integration program of the two video cameras. The water flow field does not reflect the whole wide cross-section of river, so it is not intuitive.

Taking the ideas of Tang [4] and Zhang [5-7], we propose a dual-camera LSPIV system which is based on two digital video cameras on bridge. Each video camera captures more than half of the wide cross-section river surface, and then the two video images are stitched into one covering the entire river, which solves the problem of the single-camera's resolution. The experimental results show that the proposed dual-camera LSPIV system effectively improves the vector accuracy of the far-field.

This paper is organized as follows. Section 2 describes the measurement device. Section 3 describes the dual-camera LSPIV system including image acquisition, image stitching, and motion estimation. Section 4 shows the experimental results of the system. Section 5 summarizes the main ideas of this paper and gives suggestions for further research.

2. Measuring Devices

The measurement devices of shore-based LSPIV system consist of a commercially available digital IP video camera, a Power on Ethernet (PoE) switcher, and a host PC, as illustrated in Fig. 1. The IP video camera captures the video images and transfers the images to the PoE switcher. The PoE switcher provides power to the video camera and transfers the images to the host PC. Relative to the shore-based LSPIV system, the proposed dual-camera based LSPIV system, illustrated in Fig. 2, has two digital IP video cameras, and the other devices are identical.

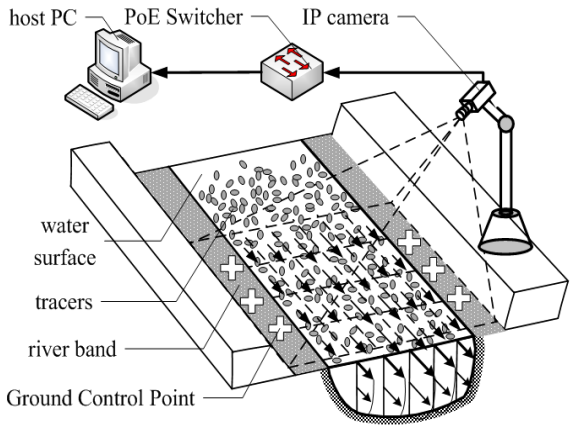

Fig. 1. Schematic of shore-based LSPIV system.

The IP video camera was WAPA BL-720Q [8]. It takes a Megapixel WDR CMOS (MT9M033) as the image sensor. With wide spectral response range (400-1050 nm), wide dynamic range (120 dB), and high sensitivity (6.0 V/lux-sec), the sensor compensates well for the low illumination condition due to the intensity loss of visible band in our LSPIV system. There was an IR-cut filter mounted on the sensor surface to recover the reality scenes of human vision percept.

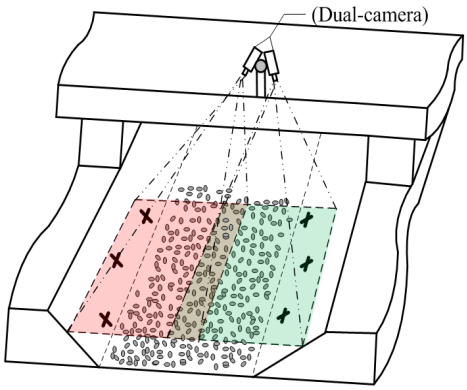

Fig. 2. Schematic of dual-camera LSPIV system.

The two video cameras were connected to a 4-port PoE switcher (WAPA BL-S104) which was powered by 48 VDC. The images which are captured from the two cameras are directly uploaded to a host PC through the PoE switcher and processed with the LSPIV system which will be described in Section 3.

In this study, we mainly focus on the image stitching and motion estimation. So the captured images didn't cover ground control points. It is enough to verify the feasibility and effectiveness of the dual-camera based LSPIV system.

3. LSPIV System

The developed dual-camera based LSPIV system can be divided into three modules: image acquisition, image stitching, and motion estimation, as show in Fig. 3.

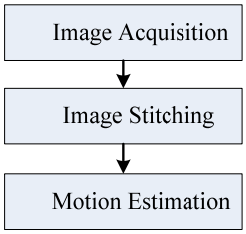

Fig. 3. Architecture of the dual-camera LSPIV system.

3.1. Image Acquisition

The image acquisition module is responsible for controlling the IP video camera, including the connection of camera, the configuration of imaging parameters (e.g. resolution and gains), as well as the selection of storage path and format.

The two cameras connect to the PoE switcher and the PoE switcher connects to the host PC. The camera simultaneously outputs two kinds of real-time media [9], a compressed video stream with MPEG-4 format and an uncompressed image stream with YUV format. The resolution can be selected between 1280×960 pixels and 960×720 pixels. The normal frame rate is 25 frames per second (fps). In poor illumination conditions, it will be reduced to extend the exposure time. This situation should be avoided, since it disorders the time interval of image pairs, which is assumed to be a known constant.

In order to avoid the image degradation caused by video compression [10], only the intensity component Y of the uncompressed YUV image stream is extracted to get grayscale images. Since the host PC passively receives frames from the camera, the frame rate of 25 fps cannot be changed. Moreover, capturing new frame while processing the previous one will require great calculating ability for the host PC, otherwise, some frames may be dropped. Aiming at solving these problems, every frame is time-stamped with the system clock and the series number in capturing order to judge the temporal validity of captured sequence. And an alternative way is adopted by setting a frame counter to check whether the image capturing process is over or not. In this system, we controlled the synchronization of the two video signals by the means of software. Only the image acquisitioned by the same time could be stitched.

3.2. Image Stitching

The image stitching module is applied to stitch the two video images acquisitioned simultaneously into a high-resolution image of the wide cross-section river, making up the defects of classic shore-based LSPIV system.

This paper takes a matching method based on SIFT (Scale-invariant feature transform) [11] feature point, because the SIFT feature points has good robustness with scale invariance, rotational invariance, brightness unknown sense. And we can get much more SIFT feature points than any other algorithms for the same image.

Video image stitching algorithm based on SIFT includes the following steps illustrated in Fig. 4.

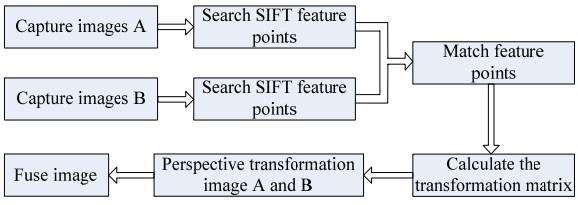

Fig. 4. Image stitching technology framework based on feature points.

Step 1: Get two images captured the same time separately from the left and the right video camera; then, search for the SIFT feature points in the two images [12].

The SIFT features are invariant to image scaling, translation, and rotation, and partially invariant to illumination changes and affine or 3D projection. These features share similar properties with neurons in inferior temporal cortex that are used for object recognition in primate vision. Features are efficiently detected through a staged filtering approach that identifies stable points in scale space.

Step 2: Describe the SIFT feature points using descriptor [13]. The original SIFT operator descriptor has 128 dimensions. In order to improve the system's efficiency, we presents an optimization algorithm to a 32-dimensional simplified SIFT descriptor.

Step 3: Match the feature points descriptor in the two images by minimum Euclidean distance [14]; set a ratio threshold between the minimum Euclidean distance and the second smallest Euclidean distance to remove he not obvious feature points.

Step 4: Previous, we matched the feature points. Now calculate 8 parameters perspective transformation matrix by at least 4 pairs feature points [15]. Transform the spatial position in the time domain of the two images.

Step 5: After the time-domain transform, stitch the two images into a wide cross-section image covering the entire river.

3.3. Motion Estimation

Motion estimation module uses the Fast Fourier Transform Cross-Correlation (FFT-CC) algorithm [16] to estimate the instantaneous displacement field. It substitutes matrix convolution in spatial domain for matrix multiplication in frequency domain to simplify and significantly speed up the cross-correlation [17-18] process. FFT-CC takes advantage of the correlation theorem which states that the Fourier transform of two functions' cross-correlation is the complex conjugate multiplication of their Fourier transforms, as shown in Equation (1):

$$c = ifft2\{fft2(A) \times conj[fft2(B)]\} \quad (1)$$

Fig. 5 illustrates the implementation of the FFT-CC algorithm. Firstly, read two successive frames from the captured image sequence as the image pair to process. Secondly, divide each image into small interrogation areas (denoted as Area a and Area b, respectively) with the same size which depends on the flow velocity and the time interval Δt . In practical, for a window size of length k , a third of this length ($k/3$) is an adequate limit to estimate the displacement vector. Thirdly, calculate the correlation function c with 2D matrix A and B by Equation (1). Finally, detect the peak value in the two-dimensional correlation plane. The corresponding coordinates will be the average displacement in the interrogation area.

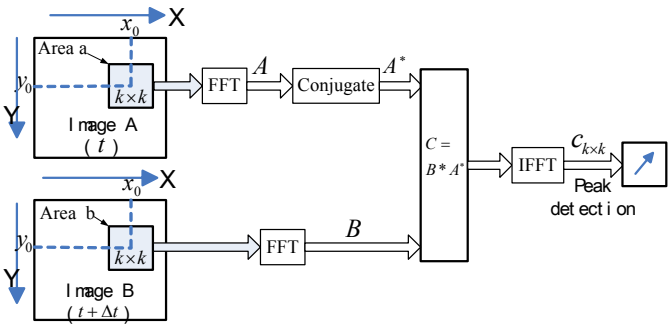

Fig. 5. Schematic diagram of FFT-CC algorithm.

4. Experimental Results

4.1. Experimental Location

The experimental location was conducted at the Yang-Chen Bridge on Niushoushan River which is nearby Hohai University in Nanjing as illustrated in Fig. 6 (a) and Fig. 6 (b).

(a) Aerial view (b) Camera equipment view

(c) Camera layout

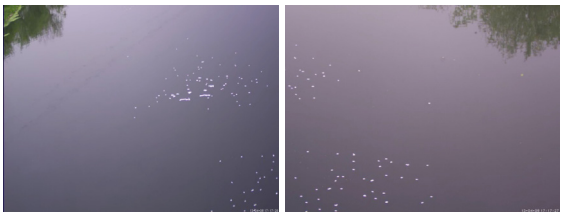

(d) Left view (e) Right view

Fig. 6. FOVs of experimental location.

The cross-section of the river is about 24 m in width, with a slant, gentle flow and uniformly distributed velocity. As the surface of the water has no enough particles for feature detection, we need to seed some proper artificial particles. In dry season, the water depth is about 0.7 m, and the average velocity in middle stream is less than 0.3 m/s. In flood season, the maximum velocity is about 1.5 m/s. Our LSPIV system was set on the bridge of the river. The angle between optical axis and water surface was 45 degrees. The angle between the two optical axes is 30 degrees, as illustrated in Fig. 6 (c).

Fig. 6 (d) is the image captured from the left video camera; Fig. 6 (e) is the image captured from the right video camera.

4.2. Image Stitching Results

According to the section 3.2 image stitching model, firstly, we look for SIFT feature points in the two images. Found 312 feature points as illustrated in Fig. 7 (a) on the left image and 217 feature points as illustrated in Fig. 7 (b) on the right one.

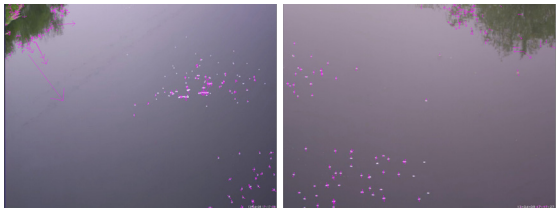

(a) Left image (b) Right image

Fig. 7. Located feature points.

Then, match the feature points based on the criterion of minimum Euclidean distance, finding 13 pairs of correct matching feature points as illustrated in Fig. 8. And compute 8 parameters of the perspective transformation model between the two images. Finally Fig. 9 is the stitching result.

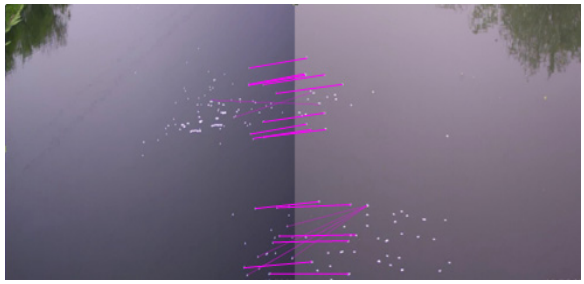

Fig. 8. Match the SIFT feature points.

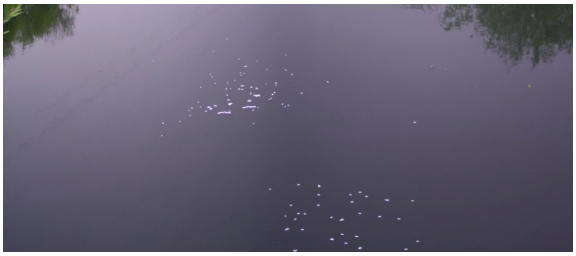

Fig. 9. Stitching result.

4.3. Motion Estimation Results

According to the motion estimation module discussed in 3.4, we take two images with 0.4 s time interval (10 frames) to calculate the flow field like Fig. 10. From the image, we can find that the higher the concentration of particles, the more accurate the flow field.

In order to emphasize the advantages of the designed dual-camera based LSPIV for the wide cross-section river flow velocity measurement proposed by this paper; we filmed a short video on the river bank by shore-based type. Estimate the motion using FFT-CC, obtained as Fig. 11.

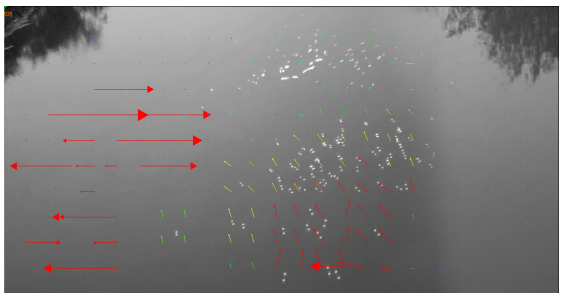

Fig. 10. Motion estimation of stitched image.

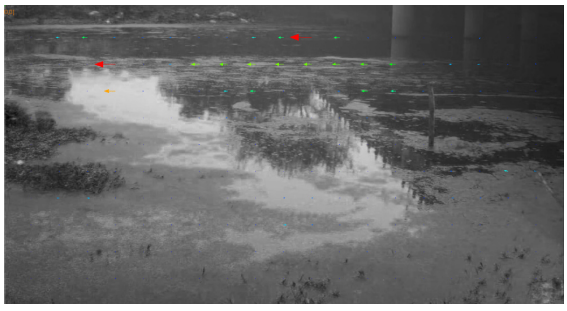

Fig. 11. Motion estimation of shore-based type.

From Fig. 11 we can find that the images collected are lack of details, due to the limit of resolution by using one single IP video camera. So it can't fully reflect the river flow filed information. By contrast, the proposed dual-camera based LSPIV can get high-resolution surface images by stitching two camera images into one image shown in Fig. 9 and get more flow filed picture like Fig. 10.

Due to the lack of resolution of the far field, the images collected by shore-based LSPIV system have a more accurate flow rate as 95.6 % in the near filed, but the far field has the lower resolution as 20.4 % and the vector error is dramatically larger as the distance increases.

The dual-camera LSPIV system proposed in this paper gets higher resolution images. It not only makes the vector accuracy reaching 95 % in the river's center, but also ensures vector accuracy reach to 82 % in both the two sides of the river as illustrated in Table 1.

5. Conclusions

In order to improve the accuracy of the vectors in the far-field of the conventional LSPIV system, a dual-camera based LSPIV system has been developed. The system is based on two digital IP video cameras. Images captured by the two cameras are analyzed and stitched into one wide cross-section image by the proposed LSPIV system. The stitched images have a higher resolution in the far-field, which meets the requirement to complete the velocimetry task. In the far field of system, the accuracy of the vector increases from 20.4 % to 80.4 %.

With the development of smart camera, many high performance video cameras will be produced. They will significantly improve multi-camera LSPIV resolution, and real-time processing capabilities. In future work, we will further study the ground control points calibration and the flow field post processing.

Acknowledgements

This study is supported by the National Natural Science Foundation of China (No. 61263029), Youth Foundation of Nanjing Institute of Technology, China (No. QKJA201204).

Table 1. Comparison of the vector accuracy between shore-based and dual-camera system.

Spatial resolution (m)	0-3	3-6	6-9	9-12	12-15	15-18	18-21	21-24
Shore-based (%)	95.6	86.3	74.2	63.1	52.6	42.1	31.5	20.4
Dual-camera (%)	82.5	87.5	91.7	95.7	95.8	91.4	87.6	82.4

References

[1]. I. Fujita, M. Muste, A. Kruger, Large-scale particle image velocimetry for flow analysis in hydraulic engineering applications, *Journal of Hydraulic Research*, Vol. 36, Issue 3, 1998, pp. 397-414.

[2]. I. Fujita, Y. Kunita, Application of aerial LSPIV to the 2002 flood of the Yodo River using a helicopter mounted high density video camera, *Journal of Hydro-environment Research*, Vol. 5, Issue 4, 2011, pp. 323-331.

[3]. A. Bechle, C. Wu, W. Liu, *et al*., Development and application of an automated river-estuary discharge imaging system, *Journal of Hydraulic Engineering*, Vol. 138, Issue 4, 2011, pp. 327-339.

[4]. H. Tang, C. Chen, H. Chen, *et al.*, An improved PTV system for large-scale physical river model, *Journal of Hydrodynamics, Ser. B*, Vol. 20, Issue 6, 2008, pp. 669-678.

[5]. Z. Zhang, L. Xu, H. Han, X. Yan, RBFNN model-based discharge soft-sensing method for open channel, *Chinese Journal of Scientific Instrument,* Vol. 32, Issue 12, 2011, pp. 2648-2654.

[6]. Z. Zhang, X. Wang, T. Fan, L. Xu, River surface target enhancement and background suppression for unseeded LSPIV, *Flow Measurement and Instrumentation,* Vol. 30, 2013, pp. 99-111.

[7]. Z. Zhang, X. Yan, T. Fan, X. Wang, L. Xu, Portable large-scale particle image velocimeter based on NIR imaging. *Chinese Journal of Scientific Instrument*, Vol. 33, Issue 12, 2012, pp. 2840-2850.

[8]. L. Xu, X. Li, S. Yang, Intelligent Information Processing and System Optimization, *Intelligent Automation and Soft Computing*, Vol. 17, Issue 7, 2011, pp. 829-833.

[9]. L. Xu, M. Li, A. Shi, M. Tang, F. Huang, Feature detector model for multi-spectral remote sensing image inspired by insect visual system, *Acta Electronica Sinic*, Vol. 39, Issue 11, 2011, pp. 2497-2501.

[10]. G. Hu, L. Xu, M. Jin, Reliability Testing for Blind Processing Results of LFM Signals Based on NP Criterion, *Acta Electronic Sinica,* Vol. 41, Issue 4, 2013, pp. 739-743.

[11]. D. Lowe, Object recognition from local scale-invariant features, *Proceedings of the 7th IEEE International Conference on Computer Vision*, Vol. 2, 1999, pp. 1150-1157.

[12]. G. Tan, X. Ni, X. Liu, *et al*., Real-Time Multicast With Network Coding In Mobile Ad-Hoc Networks, *Intelligent Automation & Soft Computing*, Vol. 18, Issue 7, 2012, pp. 783-794.

[13]. A. Shi, L. Xu, F. Xu, *et al.*, Multispectral and panchromatic image fusion based on improved bilateral filter, *Journal of Applied Remote Sensing*, Vol. 5, Issue 1, 2011, p. 053542.

[14]. G. Tan, Y. Li, An Adaptive HEC Scheme with Variable Packet Size for Wireless Real-time Reliable Multicast, *Chinese Journal of Electronics*, Vol. 21, Issue 2, 2012, pp. 299-303.

[15]. F. Huang, M. Li, A. Shi, M. Tang, L. Xu, Insect visual system inspired small target detection for multi-spectral remotely sensed images, *Journal on Communications*, Vol. 32, Issue 9, 2011, pp. 88-95.

[16]. C. Willert, M. Gharib, Digital particle image velocimetry, *Experiments in Fluids,* Vol. 10, Issue 4, 1991, pp. 181-193.

[17]. H. Wang, Z. Chen, X. Wang, Y. Ma, Random finite sets based UPF-CPHD multi-object tracking, *Journal on Communications,* 2012, Vol. 33, Issue 12, pp. 147-153.

[18]. M. Xu, F. Xu, C. Huang, M. Li, Image restoration using majorization-minimizaiton algorithm based on generalized total variation, *Journal of Image and Graphics*, Vol. 16, Issue 7, 2011, pp. 1317- 1325.